Production of Σ^0 and Ω^- in Z decays

W. Adam, T. Adye, E. Agasi, I. Ajinenko, R. Aleksan, G D. Alekseev, R. Alemany, P P. Allport, S. Almehed, U. Amaldi, et al.

EUROPEAN ORGANIZATION FOR NUCLEAR RESEARCH

CERN–PPE/96-12

31 January 1996

Production of Σ^0 and Ω^- in Z Decays

DELPHI Collaboration

Abstract

Reconstructed Λ baryon decays and photon conversions in DELPHI are used to measure the Σ^0 production rate from hadronic Z^0 decays at LEP. The number of Σ^0 decays per hadronic Z decay is found to be:

$$< \Sigma^0 + \overline{\Sigma}^0 >= 0.070 \pm 0.010\ (stat.)\ \pm 0.010\ (syst.)\ .$$

The Ω^- production rate is similarly measured to be:

$$< \Omega^- + \overline{\Omega}^+ >= 0.0014 \pm 0.0002\ (stat.)\ \pm 0.0004\ (syst.)$$

by a combination of methods using constrained fits to the whole decay chain and particle identification.

(To be submitted to Zeit f. Physik C.)

W.Adam[50], T.Adye[37], E.Agasi[31], I.Ajinenko[42], R.Aleksan[39], G.D.Alekseev[16], R.Alemany[49], P.P.Allport[22], S.Almehed[24], U.Amaldi[9], S.Amato[47], A.Andreazza[28], M.L.Andrieux[14], P.Antilogus[9], W-D.Apel[17], Y.Arnoud[39], B.Åsman[44], J-E.Augustin[19], A.Augustinus[9], P.Baillon[9], P.Bambade[19], F.Barao[21], R.Barate[14], M.Barbi[47], D.Y.Bardin[16], A.Baroncelli[40], O.Barring[24], J.A.Barrio[26], W.Bartl[50], M.J.Bates[37], M.Battaglia[15], M.Baubillier[23], J.Baudot[39], K-H.Becks[52], M.Begalli[6], P.Beilliere[8], Yu.Belokopytov[9,53], K.Beloous[42], A.C.Benvenuti[5], M.Berggren[47], D.Bertrand[2], F.Bianchi[45], M.Bigi[45], M.S.Bilenky[16], P.Billoir[23], D.Bloch[10], M.Blume[52], S.Blyth[35], T.Bolognese[39], M.Bonesini[28], W.Bonivento[28], P.S.L.Booth[22], G.Borisov[42], C.Bosio[40], S.Bosworth[35], O.Botner[48], E.Boudinov[31], B.Bouquet[19], C.Bourdarios[9], T.J.V.Bowcock[22], M.Bozzo[13], P.Branchini[40], K.D.Brand[36], T.Brenke[52], R.A.Brenner[15], C.Bricman[2], L.Brillault[23], R.C.A.Brown[9], P.Bruckman[18], J-M.Brunet[8], L.Bugge[33], T.Buran[33], T.Burgsmueller[52], P.Buschmann[52], A.Buys[9], S.Cabrera[49], M.Caccia[28], M.Calvi[28], A.J.Camacho Rozas[41], T.Camporesi[9], V.Canale[38], M.Canepa[13], K.Cankocak[44], F.Cao[2], F.Carena[9], L.Carroll[22], C.Caso[13], M.V.Castillo Gimenez[49], A.Cattai[9], F.R.Cavallo[5], L.Cerrito[38], V.Chabaud[9], M.Chapkin[42], Ph.Charpentier[9], L.Chaussard[25], J.Chauveau[23], P.Checchia[36], G.A.Chelkov[16], M.Chen[2], R.Chierici[45], P.Chliapnikov[42], P.Chochula[7], V.Chorowicz[9], J.Chudoba[30], V.Cindro[43], P.Collins[9], J.L.Contreras[19], R.Contri[13], E.Cortina[49], G.Cosme[19], F.Cossutti[46], H.B.Crawley[1], D.Crennell[37], G.Crosetti[13], J.Cuevas Maestro[34], S.Czellar[15], E.Dahl-Jensen[29], J.Dahm[52], B.Dalmagne[19], M.Dam[29], G.Damgaard[29], P.D.Dauncey[37], M.Davenport[9], W.Da Silva[23], C.Defoix[8], A.Deghorain[2], G.Della Ricca[46], P.Delpierre[27], N.Demaria[35], A.De Angelis[9], W.De Boer[17], S.De Brabandere[2], C.De Clercq[2], C.De La Vaissiere[23], B.De Lotto[46], A.De Min[36], L.De Paula[47], C.De Saint-Jean[39], H.Dijkstra[9], L.Di Ciaccio[38], F.Djama[10], J.Dolbeau[8], M.Donszelmann[9], K.Doroba[51], M.Dracos[10], J.Drees[52], K.-A.Drees[52], M.Dris[32], Y.Dufour[9], D.Edsall[1], R.Ehret[17], G.Eigen[4], T.Ekelof[48], G.Ekspong[44], M.Elsing[52], J-P.Engel[10], N.Ershaidat[23], B.Erzen[43], M.Espirito Santo[21], E.Falk[24], D.Fassouliotis[32], M.Feindt[9], A.Ferrer[49], T.A.Filippas[32], A.Firestone[1], P.-A.Fischer[10], H.Foeth[9], E.Fokitis[32], F.Fontanelli[13], F.Formenti[9], B.Franek[37], P.Frenkiel[8], D.C.Fries[17], A.G.Frodesen[4], R.Fruhwirth[50], F.Fulda-Quenzer[19], J.Fuster[49], A.Galloni[22], D.Gamba[45], M.Gandelman[6], C.Garcia[49], J.Garcia[41], C.Gaspar[9], U.Gasparini[36], Ph.Gavillet[9], E.N.Gazis[32], D.Gele[10], J-P.Gerber[10], L.Gerdyukov[42], M.Gibbs[22], R.Gokieli[51], B.Golob[43], G.Gopal[37], L.Gorn[1], M.Gorski[51], Yu.Gouz[45,53], V.Gracco[13], E.Graziani[40], G.Grosdidier[19], K.Grzelak[51], S.Gumenyuk[28,53], P.Gunnarsson[44], M.Gunther[48], J.Guy[37], F.Hahn[9], S.Hahn[52], A.Hallgren[48], K.Hamacher[52], W.Hao[31], F.J.Harris[35], V.Hedberg[24], R.Henriques[21], J.J.Hernandez[49], P.Herquet[2], H.Herr[9], T.L.Hessing[35], E.Higon[49], H.J.Hilke[9], T.S.Hill[1], S-O.Holmgren[44], P.J.Holt[35], D.Holthuizen[31], S.Hoorelbeke[2], M.Houlden[22], J.Hrubec[50], K.Huet[2], K.Hultqvist[44], J.N.Jackson[22], R.Jacobsson[44], P.Jalocha[18], R.Janik[7], Ch.Jarlskog[24], G.Jarlskog[24], P.Jarry[39], B.Jean-Marie[19], E.K.Johansson[44], L.Jonsson[24], P.Jonsson[24], C.Joram[9], P.Juillot[10], M.Kaiser[17], F.Kapusta[23], K.Karafasoulis[11], M.Karlsson[44], E.Karvelas[11], S.Katsanevas[3], E.C.Katsoufis[32], R.Keranen[4], B.A.Khomenko[16], N.N.Khovanski[16], B.King[22], N.J.Kjaer[29], H.Klein[9], A.Klovning[4], P.Kluit[31], B.Koene[31], P.Kokkinias[11], M.Koratzinos[9], K.Korcyl[18], V.Kostioukhine[42], C.Kourkoumelis[3], O.Kouznetsov[13,16], P.-H.Kramer[52], M.Krammer[50], C.Kreuter[17], I.Kronkvist[24], Z.Krumstein[16], W.Krupinski[18], P.Kubinec[7], W.Kucewicz[18], K.Kurvinen[15], C.Lacasta[49], I.Laktineh[25], S.Lamblot[23], J.W.Lamsa[1], L.Lanceri[46], D.W.Lane[1], P.Langefeld[52], I.Last[22], J-P.Laugier[39], R.Lauhakangas[15], G.Leder[50], F.Ledroit[14], V.Lefebure[2], C.K.Legan[1], R.Leitner[30], Y.Lemoigne[39], J.Lemonne[2], G.Lenzen[52], V.Lepeltier[19], T.Lesiak[36], D.Liko[50], R.Lindner[52], A.Lipniacka[36], I.Lippi[36], B.Loerstad[24], J.G.Loken[35], J.M.Lopez[41], D.Loukas[11], P.Lutz[39], L.Lyons[35], J.MacNaughton[50], G.Maehlum[17], A.Maio[21], V.Malychev[16], F.Mandl[50], J.Marco[41], R.Marco[41], B.Marechal[47], M.Margoni[36], J-C.Marin[9], C.Mariotti[40], A.Markou[11], T.Maron[52], C.Martinez-Rivero[41], F.Martinez-Vidal[49], S.Marti i Garcia[49], J.Masik[30], F.Matorras[41], C.Matteuzzi[9], G.Matthiae[38], M.Mazzucato[36], M.Mc Cubbin[9], R.Mc Kay[1], R.Mc Nulty[22], J.Medbo[48], M.Merk[31], C.Meroni[28], S.Meyer[17], W.T.Meyer[1], M.Michelotto[36], E.Migliore[45], L.Mirabito[25], W.A.Mitaroff[50], U.Mjoernmark[24], T.Moa[44], R.Moeller[29], K.Moenig[9], M.R.Monge[13], P.Morettini[13], H.Mueller[17], L.M.Mundim[6], W.J.Murray[37], B.Muryn[18], G.Myatt[35], F.Naraghi[14], F.L.Navarria[5], S.Navas[49], K.Nawrocki[51], P.Negri[28], W.Neumann[52], N.Neumeister[50], R.Nicolaidou[3], B.S.Nielsen[29], M.Nieuwenhuizen[31], V.Nikolaenko[10], P.Niss[44], A.Nomerotski[36], A.Normand[35], W.Oberschulte-Beckmann[17], V.Obraztsov[42], A.G.Olshevski[16], A.Onofre[21], R.Orava[15], K.Osterberg[15], A.Ouraou[39], P.Paganini[19], M.Paganoni[9], P.Pages[10], H.Palka[18], Th.D.Papadopoulou[32], K.Papageorgiou[11], L.Pape[9], C.Parkes[35], F.Parodi[13], A.Passeri[40], M.Pegoraro[36], L.Peralta[21], H.Pernegger[50], M.Pernicka[50], A.Perrotta[5], C.Petridou[46], A.Petrolini[13], M.Petrovyck[28,53], H.T.Phillips[37], G.Piana[13], F.Pierre[39], M.Pimenta[21], M.Pindo[28], S.Plaszczynski[19], O.Podobrin[17], M.E.Pol[6], G.Polok[18], P.Poropat[46], V.Pozdniakov[16], M.Prest[46], P.Privitera[38], N.Pukhaeva[16], A.Pullia[28], D.Radojicic[35], S.Ragazzi[28], H.Rahmani[32], J.Rames[12], P.N.Ratoff[20], A.L.Read[33], M.Reale[52], P.Rebecchi[19], N.G.Redaelli[28], D.Reid[9], P.B.Renton[35], L.K.Resvanis[3], F.Richard[19], J.Richardson[22], J.Ridky[12], G.Rinaudo[45], I.Ripp[39], A.Romero[45], I.Roncagliolo[13], P.Ronchese[36], L.Roos[14], E.I.Rosenberg[1], E.Rosso[9], P.Roudeau[19], T.Rovelli[5], W.Ruckstuhl[31], V.Ruhlmann-Kleider[39], A.Ruiz[41], K.Rybicki[18], H.Saarikko[15], Y.Sacquin[39], A.Sadovsky[16], G.Sajot[14], J.Salt[49], J.Sanchez[26], M.Sannino[13], M.Schimmelpfennig[17], H.Schneider[17], U.Schwickerath[17], M.A.E.Schyns[52], G.Sciolla[45], F.Scuri[46], P.Seager[20], Y.Sedykh[16], A.M.Segar[35], A.Seitz[17], R.Sekulin[37], R.C.Shellard[6], I.Siccama[31], P.Siegrist[39], S.Simonetti[39], F.Simonetto[36], A.N.Sisakian[16], B.Sitar[7], T.B.Skaali[33], G.Smadja[25], N.Smirnov[42], O.Smirnova[16], G.R.Smith[37], O.Solovianov[42], R.Sosnowski[51], D.Souza-Santos[6], T.Spassov[21], E.Spiriti[40], P.Sponholz[52], S.Squarcia[13], C.Stanescu[40], S.Stapnes[33], I.Stavitski[36], F.Stichelbaut[9], A.Stocchi[19], J.Strauss[50], R.Strub[10], B.Stugu[4], M.Szczekowski[51], M.Szeptycka[51], T.Tabarelli[28],

J.P.Tavernet[23], O.Tchikilev[42], A.Tilquin[27], J.Timmermans[31], L.G.Tkatchev[16], T.Todorov[10], D.Z.Toet[31], A.Tomaradze[2], B.Tome[21], A.Tonazzo[28], L.Tortora[40], G.Transtromer[24], D.Treille[9], W.Trischuk[9], G.Tristram[8], A.Trombini[19], C.Troncon[28], A.Tsirou[9], M-L.Turluer[39], I.A.Tyapkin[16], M.Tyndel[37], S.Tzamarias[22], B.Ueberschaer[52], O.Ullaland[9], V.Uvarov[42], G.Valenti[5], E.Vallazza[9], C.Vander Velde[2], G.W.Van Apeldoorn[31], P.Van Dam[31], W.K.Van Doninck[2], J.Van Eldik[31], N.Vassilopoulos[35], G.Vegni[28], L.Ventura[36], W.Venus[37], F.Verbeure[2], M.Verlato[36], L.S.Vertogradov[16], D.Vilanova[39], P.Vincent[25], L.Vitale[46], E.Vlasov[42], A.S.Vodopyanov[16], V.Vrba[12], H.Wahlen[52], C.Walck[44], F.Waldner[46], M.Weierstall[52], P.Weilhammer[9], C.Weiser[17], A.M.Wetherell[9], D.Wicke[52], J.H.Wickens[2], M.Wielers[17], G.R.Wilkinson[35], W.S.C.Williams[35], M.Winter[10], K.Woschnagg[48], K.Yip[35], O.Yushchenko[42], F.Zach[25], A.Zaitsev[42], A.Zalewska[18], P.Zalewski[51], D.Zavrtanik[43], E.Zevgolatakos[11], N.I.Zimin[16], M.Zito[39], D.Zontar[43], R.Zuberi[35], G.C.Zucchelli[44], G.Zumerle[36]

[1] Ames Laboratory and Department of Physics, Iowa State University, Ames IA 50011, USA
[2] Physics Department, Univ. Instelling Antwerpen, Universiteitsplein 1, B-2610 Wilrijk, Belgium
and IIHE, ULB-VUB, Pleinlaan 2, B-1050 Brussels, Belgium
and Faculté des Sciences, Univ. de l'Etat Mons, Av. Maistriau 19, B-7000 Mons, Belgium
[3] Physics Laboratory, University of Athens, Solonos Str. 104, GR-10680 Athens, Greece
[4] Department of Physics, University of Bergen, Allégaten 55, N-5007 Bergen, Norway
[5] Dipartimento di Fisica, Università di Bologna and INFN, Via Irnerio 46, I-40126 Bologna, Italy
[6] Centro Brasileiro de Pesquisas Físicas, rua Xavier Sigaud 150, RJ-22290 Rio de Janeiro, Brazil
and Depto. de Física, Pont. Univ. Católica, C.P. 38071 RJ-22453 Rio de Janeiro, Brazil
and Inst. de Física, Univ. Estadual do Rio de Janeiro, rua São Francisco Xavier 524, Rio de Janeiro, Brazil
[7] Comenius University, Faculty of Mathematics and Physics, Mlynska Dolina, SK-84215 Bratislava, Slovakia
[8] Collège de France, Lab. de Physique Corpusculaire, IN2P3-CNRS, F-75231 Paris Cedex 05, France
[9] CERN, CH-1211 Geneva 23, Switzerland
[10] Centre de Recherche Nucléaire, IN2P3 - CNRS/ULP - BP20, F-67037 Strasbourg Cedex, France
[11] Institute of Nuclear Physics, N.C.S.R. Demokritos, P.O. Box 60228, GR-15310 Athens, Greece
[12] FZU, Inst. of Physics of the C.A.S. High Energy Physics Division, Na Slovance 2, 180 40, Praha 8, Czech Republic
[13] Dipartimento di Fisica, Università di Genova and INFN, Via Dodecaneso 33, I-16146 Genova, Italy
[14] Institut des Sciences Nucléaires, IN2P3-CNRS, Université de Grenoble 1, F-38026 Grenoble Cedex, France
[15] Research Institute for High Energy Physics, SEFT, P.O. Box 9, FIN-00014 Helsinki, Finland
[16] Joint Institute for Nuclear Research, Dubna, Head Post Office, P.O. Box 79, 101 000 Moscow, Russian Federation
[17] Institut für Experimentelle Kernphysik, Universität Karlsruhe, Postfach 6980, D-76128 Karlsruhe, Germany
[18] Institute of Nuclear Physics and University of Mining and Metalurgy, Ul. Kawiory 26a, PL-30055 Krakow, Poland
[19] Université de Paris-Sud, Lab. de l'Accélérateur Linéaire, IN2P3-CNRS, Bât. 200, F-91405 Orsay Cedex, France
[20] School of Physics and Materials, University of Lancaster, Lancaster LA1 4YB, UK
[21] LIP, IST, FCUL - Av. Elias Garcia, 14-1^{o}, P-1000 Lisboa Codex, Portugal
[22] Department of Physics, University of Liverpool, P.O. Box 147, Liverpool L69 3BX, UK
[23] LPNHE, IN2P3-CNRS, Universités Paris VI et VII, Tour 33 (RdC), 4 place Jussieu, F-75252 Paris Cedex 05, France
[24] Department of Physics, University of Lund, Sölvegatan 14, S-22363 Lund, Sweden
[25] Université Claude Bernard de Lyon, IPNL, IN2P3-CNRS, F-69622 Villeurbanne Cedex, France
[26] Universidad Complutense, Avda. Complutense s/n, E-28040 Madrid, Spain
[27] Univ. d'Aix - Marseille II - CPP, IN2P3-CNRS, F-13288 Marseille Cedex 09, France
[28] Dipartimento di Fisica, Università di Milano and INFN, Via Celoria 16, I-20133 Milan, Italy
[29] Niels Bohr Institute, Blegdamsvej 17, DK-2100 Copenhagen 0, Denmark
[30] NC, Nuclear Centre of MFF, Charles University, Areal MFF, V Holesovickach 2, 180 00, Praha 8, Czech Republic
[31] NIKHEF-H, Postbus 41882, NL-1009 DB Amsterdam, The Netherlands
[32] National Technical University, Physics Department, Zografou Campus, GR-15773 Athens, Greece
[33] Physics Department, University of Oslo, Blindern, N-1000 Oslo 3, Norway
[34] Dpto. Fisica, Univ. Oviedo, C/P. Pérez Casas, S/N-33006 Oviedo, Spain
[35] Department of Physics, University of Oxford, Keble Road, Oxford OX1 3RH, UK
[36] Dipartimento di Fisica, Università di Padova and INFN, Via Marzolo 8, I-35131 Padua, Italy
[37] Rutherford Appleton Laboratory, Chilton, Didcot OX11 OQX, UK
[38] Dipartimento di Fisica, Università di Roma II and INFN, Tor Vergata, I-00173 Rome, Italy
[39] Centre d'Etudes de Saclay, DSM/DAPNIA, F-91191 Gif-sur-Yvette Cedex, France
[40] Istituto Superiore di Sanità, Ist. Naz. di Fisica Nucl. (INFN), Viale Regina Elena 299, I-00161 Rome, Italy
[41] Instituto de Fisica de Cantabria (CSIC-UC), Avda. los Castros, S/N-39006 Santander, Spain, (CICYT-AEN93-0832)
[42] Inst. for High Energy Physics, Serpukov P.O. Box 35, Protvino, (Moscow Region), Russian Federation
[43] J. Stefan Institute and Department of Physics, University of Ljubljana, Jamova 39, SI-61000 Ljubljana, Slovenia
[44] Fysikum, Stockholm University, Box 6730, S-113 85 Stockholm, Sweden
[45] Dipartimento di Fisica Sperimentale, Università di Torino and INFN, Via P. Giuria 1, I-10125 Turin, Italy
[46] Dipartimento di Fisica, Università di Trieste and INFN, Via A. Valerio 2, I-34127 Trieste, Italy
and Istituto di Fisica, Università di Udine, I-33100 Udine, Italy
[47] Univ. Federal do Rio de Janeiro, C.P. 68528 Cidade Univ., Ilha do Fundão BR-21945-970 Rio de Janeiro, Brazil
[48] Department of Radiation Sciences, University of Uppsala, P.O. Box 535, S-751 21 Uppsala, Sweden
[49] IFIC, Valencia-CSIC, and D.F.A.M.N., U. de Valencia, Avda. Dr. Moliner 50, E-46100 Burjassot (Valencia), Spain
[50] Institut für Hochenergiephysik, Österr. Akad. d. Wissensch., Nikolsdorfergasse 18, A-1050 Vienna, Austria
[51] Inst. Nuclear Studies and University of Warsaw, Ul. Hoza 69, PL-00681 Warsaw, Poland
[52] Fachbereich Physik, University of Wuppertal, Postfach 100 127, D-42097 Wuppertal 1, Germany
[53] On leave of absence from IHEP Serpukhov

1 Introduction

Measuring the production rates of baryons in general, and strange baryons in particular, is important in order to understand the underlying fragmentation process in $Z^0 \to q\bar{q}$ events. This process has a small four-momentum transfer and perturbation theory is not applicable. Consequently, there is no good theoretical description of the phenomenon of hadronization, and one has to rely on phenomenological models. The most widely used models are implemented in the simulation programs HERWIG (cluster decay) [1] and JETSET (string fragmentation) [2]. Since there are substantial differences between these two models, a measurement of the hyperon production rates offers a possibility to gain insight into how fragmentation works.

This report describes a measurement of the production of the strange baryons[†] Σ^0 and Ω^- in Z^0 hadronic decays collected with the DELPHI detector at LEP during 1991 to 1994. The Σ^0 rate has not previously been measured at LEP energies, while Ω^- production at LEP has been measured by OPAL [3] and with more recent results presented at conferences [4,5]. The particle identification capabilities in DELPHI are used in both the Σ^0 analysis and the Ω^- analysis. In order to identify the decay $\Sigma^0 \to \Lambda\gamma$, where the Λ decays via $p\pi^-$, the Λ sample is enriched by using the RICH (Ring Imaging CHerenkov) detector to identify the proton. Photons are reconstructed from their conversion in the detector material into e^+e^- pairs. The Ω^- is studied by a complete reconstruction of the decay chain $\Omega^- \to \Lambda K^-$, where $\Lambda \to p\pi^-$. A constrained fit to the three-dimensional decay topology is used to identify the Ω^- decay and suppress the large combinatorial background. An independent analysis based on the identification of the final state kaon with the RICH detector is also performed.

As a check on the reconstruction procedure for the Ω^-, the decay of the Ξ^- hyperon is also identified ($\Xi^- \to \Lambda\pi^-$). Because of the topological resemblance of Ω^- and Ξ^- decays, the same analysis procedure is used to reconstruct the two hyperons. The large statistics makes the Ξ^- sample suitable to check the integrity of the reconstruction procedure.

Simulated events are used to optimize the analysis and selection procedures described in the following sections. The Ω^- and Σ^0 reconstruction efficiencies are evaluated by running the analysis program on the simulated events.

2 Track and Event Selection

The DELPHI detector is described in [6]. The subdetectors relevant for this analysis are the Vertex Detector (VD), the Inner Detector (ID), the Time Projection Chamber (TPC), the Outer Detector (OD) and the Ring Imaging CHerenkov detectors (RICH). The VD consists of three concentrical layers of silicon strip detectors, located at radii 6, 8 and 11 cm. The polar angle covered is $43° < \theta < 137°$, where θ is given with respect to the z-axis[‡]. In the 1994 run the first and third layer had a double-sided readout to reconstruct both $R\phi$ and z coordinates, where ϕ is the azimuthal angle and R the radial distance in the plane perpendicular to the z-axis. The TPC is the main tracking device

[†] Whenever a charged hyperon is mentioned the charge conjugated state is also referred to, unless explicitly stated otherwise.

[‡] In the standard DELPHI coordinate system, the z axis is along the electron direction, the x axis points towards the centre of LEP, and the y axis points upwards. The polar angle to the z axis is called θ and the azimuthal angle around the z axis is called ϕ; the radial coordinate is $R = \sqrt{x^2 + y^2}$.

where charged particle tracks are reconstructed in three dimensions for radii between 30 and 120 cm. The ID and OD are two drift chambers located at radii between 12 and 28 cm and between 198 and 206 cm respectively. These two detectors provide additional points for the track reconstruction. The RICH detectors are the main particle identification detectors in DELPHI. They are situated on the outside of the TPC, just in front of the OD and provide kaon and proton identification for particles in the momentum range 0.7 GeV/c to 25 GeV/c.

For the Ω^- analysis, $Z \to q\bar{q}$ events were simulated corresponding to the production of ~48,000 Ω^- hyperons in the DELPHI detector. This corresponds to ~34 million $q\bar{q}$ events. For the Σ^0 analysis, 5.3 million $Z \to q\bar{q}$ events were generated, corresponding to about 0.072 Σ^0 hyperons per hadronic event, or 382,000 Σ^0 hyperons. These simulations used the JETSET 7.3 generator with parameters tuned from previous QCD studies [7], followed by a detailed simulation of the DELPHI detector (DELSIM) [8].

A charged particle is accepted in the analysis if it has a

- track length greater than 30 cm,
- momentum larger than 100 MeV/c, and
- relative error on the momentum less than 100%.

An event is accepted as a hadronic Z^0 decay if it has

- at least 7 charged particles, each with momentum larger than 200 MeV/c,
- a total reconstructed charged energy larger than 15 GeV, calculated assuming all particles to have the pion mass,
- a total energy in charged particles of at least 3 GeV in each hemisphere (defined with respect to the beam axis) of the detector.

From the 1991 run 0.26 million events classified as hadronic Z^0 decays are selected, from the 1992 run 0.70 million events, from the 1993 run 0.71 million events, and from the 1994 run 1.39 million events.

3 The Ω^- Hyperon

The Ω^- hyperon is identified through its weak decay $\Omega^- \to \Lambda K^-$ (branching ratio $\sim 68\%$). The Λ is identified through its decay $\Lambda \to p\pi^-$ (branching ratio $\sim 64\%$). The search for an Ω^- decay is performed in two stages. First Λ candidates are found using the standard DELPHI V^0 (a V^0 is the topology for a decay of a neutral particle into two charged particles) search algorithm as will be described below. The Λ candidates are combined with charged particles of the right sign to give a candidate for the decay of an Ω^-. The huge combinatorial background is reduced by two independent methods. The first analysis uses a constrained fit to the Ω^- hypothesis, whereas the second one utilizes the RICH information to identify the kaon.

The lifetime of the Ω^- is short enough for it to decay before it is detected, in general. Therefore it has to be reconstructed using its decay products. A diagram of the Ω^- decay chain is shown in Figure 1. All decay radii are given with respect to the main vertex, which is calculated on an event by event basis.

3.1 Constrained fit method

3.1.1 Pre-selection

In the constrained fit analysis 0.67 million hadronic events were used from the 1992 run, 0.68 million from the 1993 run, and 1.24 million from the 1994 run. The standard DELPHI V^0 algorithm forms all possible pairs of tracks from oppositely charged particles in the event. A vertex fit is performed on each such pair which is then accepted as a Λ candidate if:

- the χ^2 probability of the secondary vertex fit exceeds 0.1%,
- the measured flight path in the xy-plane (the plane perpendicular to the beam axis) of the Λ candidate exceeds twice its error, and
- the angle between the momentum vector of the V^0 and the vector joining the primary and secondary vertices is less than 0.1 rad.

The invariant mass of the Λ candidate is required to be between 1.105 and 1.125 GeV/c^2 (the nominal Λ mass is 1115.684 $\pm$ 0.006 MeV/c^2 [9]). The Λ candidates are then paired with the remaining charged particles of the right sign to form Ω^- candidates. A constrained fit, described in the next paragraph, is performed if the following conditions are fulfilled when combining a Λ candidate with a charged particle:

- the charged particle is not an electron or muon,
- the projections onto the xy-plane of the Λ and charged particle trajectories intersect,
- the intersection between the Λ and charged particle trajectories is more than 8 mm away from the main vertex in the xy-plane,
- the Λ and charged particle trajectories are not more than 2 cm apart in the z direction at the point of crossing in the xy-plane.

3.1.2 The fit procedure

The specific topology of weak cascade decays makes possible a constrained fit suitable to suppress the combinatorial background. The method used is a general least squares fit with seven constraint equations. The constraints are that:

- the pion and proton from the Λ decay must intersect at the Λ decay point,
- the invariant mass of the Λ candidate has to be equal to the nominal Λ mass,
- the K^- and Λ from the Ω^- decay must intersect at the Ω^- decay point,
- momentum has to be conserved in the Ω^- decay.

There are 18 variables in the fit, 2 of them unmeasured. The two unmeasured quantities are the decay radii of the Ω^- and Λ. The measured quantities, for which the fit gives improved values, are the 5 parameters of the helix parameterization of each track and the z coordinate of the main vertex. These track parameters are: $1/R$, where R is the radius of curvature of the track, impact parameters in z and $R\phi$, the polar angle θ, and the azimuthal angle ϕ. The last four parameters are evaluated with respect to some arbitrary reference point. Since there are 3 tracks making up a Ω^- candidate, there are 16 measured variables in the fit.

All tracks are corrected for ionization losses, according to the given mass hypothesis.

The performance of the fit was tuned by adjusting the covariance matrices of the tracks. The adjustment consisted in a scaling of the errors of the track parameters. After the

adjustment the pull distributions were standard normal distributions within 10%. The adjustment was made separately for each year, because the detector setup and the reconstruction software changed with time. Since the Ω^- data sample is rather small ($\sim$100 decays) the large ($\sim$4,000 decays) Ξ^- sample was used to estimate the scaling factors.

The $\Lambda\pi^-$ invariant mass spectrum is shown in Figure 2 and exhibits a large Ξ^- signal. The Ξ^- candidates were reconstructed simultaneously with the Ω^- candidates by making the assumption that the charged particle combined with the Λ was a π^- instead of a K^-. The efficiency, including branching ratios, to reconstruct a complete Ξ^- decay chain is determined by applying the same analysis to the simulated events as to the real data, and is found to be $(5.84 \pm 0.14)\%$. From a clean sample of 3963 ± 81 reconstructed Ξ^- decays the average number of Ξ^- and $\overline{\Xi}^+$ produced per hadronic Z^0 decay is found to be

$$< \Xi^- + \overline{\Xi}^+ > = 0.0262 \pm 0.0004,$$

with only statistical error. This agrees well with our previously published result on Ξ^- production, based on a different analysis of 1991 and 1992 data [10], which is $0.0250 \pm 0.0009 \pm 0.0021$.

Figure 3 shows the agreement between the constrained fit χ^2 probability distributions for data and simulated events, after the adjustment of the covariance matrices. The same cuts were made on both data and simulation.

3.1.3 Selection of Ω^- candidates

In order to obtain a clean Ω^- signal, a rather large number of cuts must be imposed on the Ω^- candidates. The most important cut is that on the χ^2 probability of the constrained fit. Before performing the fit, the following cuts on the ΛK^- pairs are made:

- The Λ and kaon trajectories, at the point in space corresponding to the intersection in the xy-plane, are required not to be further than 7 mm apart in the z direction.
- The candidate kaon track is required to have an impact parameter with respect to the main vertex in the xy-plane of at least 0.2 mm.

After the fit, the following cuts are applied:

- The momentum of the Ω^- candidate must point into the barrel region ($|\cos\theta| < 0.85$).
- The Ω^- candidate is not allowed to have an invariant mass within ± 10 MeV/c^2 of the nominal Ξ^- mass, when the kaon track is treated as a pion.
- The χ^2 probability of the fit must be larger than 1%.
- The flight distance of the Ω^- candidate must be between 1 and 20 cm in the xy-plane.
- The radius of the Λ decay must exceed the radius of the Ω^- decay by more than 1 cm.
- The radius of the first measured point of the kaon track must not exceed the radius of the Ω^- decay by more than 40 cm.
- The maximum radii of the first measured points of the pion and proton tracks from the Λ decay are not allowed to exceed the radius of the Λ decay by more than 40 cm.
- The radius of the Λ decay point is not allowed to exceed the minimum radius of the first measured points of the pion and proton tracks by more than 3 cm.

- The cosine of the angle between the Λ and Ω^- momenta, as measured in the Ω^- rest frame must be in the interval [-0.9,0.9] (angular cut).
- The momentum of the kaon track must exceed 0.4 GeV/c.
- The momentum of the Ω^- candidate should be between 1 and 15 GeV/c.

3.1.4 Ω^- efficiency

In order to calculate the efficiency, the simulated Ω^- events are run through the same analysis chain as the real data. The efficiency is integrated over the whole momentum spectrum, meaning that the x_p distribution of Ω^- is assumed to be correctly described by JETSET . To justify this, it is noted that the agreement for Ξ^- between JETSET and data is generally good, even if the Ξ^- momentum spectrum is somewhat softer in JETSET than in data. The overall efficiency, including branching ratios, to reconstruct a complete Ω^- decay chain is determined to be $\varepsilon_{\Omega^-} = (2.56 \pm 0.07)\%$, where the error comes from the finite number of simulated Ω^- decays.

3.1.5 Systematic errors

Table 1 lists the various contributions to the systematic uncertainty.

The influence of the background parameterization of the ΛK^- invariant mass spectrum is studied. The Ω^- signal is represented by a Gaussian distribution, and the background is parameterized by first and second order polynomials. The variation in the size of the signal is taken as the systematic error due to the shape of the background.

The effect of different bin widths used for the ΛK^- invariant mass distribution on the size of the signal was examined. Bin widths of 2, 3, and 4 MeV/c^2 were tried, and the variation in the signal is taken as an estimate of the effect of binning.

In simulation $\sim$17% of the Ω^- are produced outside our momentum acceptance. The true momentum spectrum being largely unknown, we have assigned a systematic error of $\sim$8% due to unseen momentum regions (JETSET extrapolation I), and a similar uncertainty due to the shape of the momentum spectrum (JETSET extrapolation II).

Furthermore, the cuts are varied in a moderate way. In particular, the cut on the χ^2 probability of the constrained fit was the subject of detailed investigations. The distributions for data and simulation agree well, as shown in Figure 3.

Finally, there is a small contribution from the uncertainty in the reconstruction efficiency due to limited Monte Carlo statistics. For the 1992 and 1993 detector configurations, a total of 5,000 Z^0 events each containing at least one Ω^- were generated and passed through the detector simulation and event reconstruction program. For the 1994 detector configuration, an additional 10,000 Z^0 giving at least one Ω^- were generated and passed through the detector simulation and event reconstruction. These events were then analyzed in the same way as data. The simulation sample corresponds to about 48,000 Ω^- decays in total, when branching ratios are taken into account.

There are two features in the decays of Ξ^- and Ω^- that make these two hyperons very similar. They have a similar lifetime, and the Q-value of the decays are almost the same. Since the topologies of the two decay chains resemble each other, it seems plausible that a Ξ^- might easily be mistaken for an Ω^-. This depends on several features of the

Contribution from:	
Background shape	$< \pm$ 1%
Bin width	$\pm$ 5%
K^- impact parameter cut	$< \pm$ 1%
Ω^- radial flight cut	$\pm$ 13%
angular cut	$\pm$ 12%
JETSET extrapolation I	$\pm$ 8%
JETSET extrapolation II	$\pm$ 8%
χ^2 probability cut	$\pm$ 13%
Branching ratio $\Omega^- \to \Lambda K^-$	$< \pm$ 1%
Branching ratio $\Lambda \to p\pi^-$	$< \pm$ 1%
Monte Carlo statistics	$\pm$ 3%
Total	$\pm$ 25%

Table 1: Contributions to the systematic error of the Ω^- production rate measured in the constrained fit analysis.

reconstruction of the decays, the most important being the resolution of the reconstructed mass. It is seen in Figure 4 that Ξ^- decays give a flat reflexion under the Ω^- mass peak, and cannot fake an Ω^- signal. Nevertheless, reconstructed Ξ^- decays are explicitly removed by discarding those combinations which give a mass of 1.321 $\pm$ 0.010 GeV/c^2 under the Ξ^- hypothesis, as described earlier. This cut removes only (4.6 $\pm$ 0.4)% of the Ω^- sample, as can be seen in Figure 4.

3.1.6 Production of Ω^-

The ΛK^- invariant mass spectrum for the full data set is shown in Figure 5. A fit is performed in which the signal is represented by a single Gaussian with fitted mean value 1.6729 $\pm$ 0.0007 GeV/c^2. The width of the signal is 2.6 $\pm$ 0.4 MeV/c^2, fully compatible with the result obtained from simulation, 2.3 $\pm$ 0.1 MeV/c^2. The nominal Ω^- mass value is 1.67245 $\pm$ 0.00029 GeV/c^2 [9]. The possibility of systematic effects on the fitted Ω^- mass obtained above has not been studied. The background is parameterized by a function of the form $f(m) = (1 - e^{-q(m-M_{edge})})(p_0 + p_1 m)$, where M_{edge} is the sum of the Λ and K^- masses. The parameters q, p_0 and p_1 are allowed to vary freely in the fit. The fit yielded 97 $\pm$ 16 Ω^- with a signal to background ratio of about 1:1. The total inclusive Ω^- production rate is found to be

$$< \Omega^- + \overline{\Omega}^+ > = 0.0015 \pm 0.0003\ (stat.)\ \pm 0.0004\ (syst.)\ .$$

A particle/antiparticle composition of 51 $\pm$ 10 Ω^- and 46 $\pm$ 9 $\overline{\Omega}^+$ is found, which is compatible with symmetric production.

3.2 Ω^- with identified K^-

As a complement to the analysis described above, a search for the Ω^- is performed utilizing the Ring Imaging CHerenkov (RICH) detectors to identify the charged kaon coming from the Ω^- decay.

3.2.1 Selection of Ω^- candidates

For this analysis only the 1994 data is used, since in 1994 the RICH detectors were fully operational for the first time. The RICH tags used were based on likelihood probabilities for the given mass hypotheses [11].

The event selection is slightly relaxed compared to the previous analysis, giving a sample of 1.3 million events. The analysis followed the outline of the previous analysis, combining charged kaon candidate tracks with Λ candidates, except that no fit is made. The Λ candidates are found using the procedure described in section 3.1.1, and are then combined with any remaining charged particles, according to the following criteria:

- The Λ vertex must be more than 3 cm from the interaction point, measured in the xy-plane.
- The charged particle and the Λ should intersect in the xy-plane.
- The distance in the z direction between the Λ and kaon trajectories, evaluated at the crossing point in the xy-plane, had to be less than 7.5 mm.
- The crossing point should be between 1 and 20 cm from the main vertex, measured in the xy-plane.
- The momentum of the Λ should exceed 1 GeV/c.
- The invariant mass of the Λ candidate must be within 7.5 MeV/c^2 of the nominal Λ mass.
- The momentum of the charged particle should exceed 700 MeV/c, below which the RICH detectors are not sensitive.
- The transverse momentum in the candidate Ω decay is required to be below 350 MeV/c.
- To reduce the background further, the track of the Λ decay having the larger momentum (*i.e.* the proton track) is required not to be identified as a pion by the RICH.

In addition, the three track quality cuts on the position of the first measured point of the charged tracks, mentioned in section 3.1.3, are also applied.

3.2.2 Production of Ω^-

After all the preceeding cuts the charged particle was then required to be identified as a kaon by the RICH. The resultant ΛK invariant mass distribution is shown in Figure 6. Fitting the signal, as described in section 3.1.6, yields 22 ± 7 Ω^-, leaving all parameters free in the fit. The width of the signal is 2.8 ± 0.5 MeV/c^2, fully compatible with the result obtained from simulation, 3.1 ± 0.1 MeV/c^2. The efficiency, calculated from analyzing simulated events, is found to be $(1.45 \pm 0.07)\%$, giving a production yield of 0.00118 ± 0.00036, statistical error only.

The systematic uncertainty due to the Λ mass cut is estimated, by varying the cut, to be 15% . The systematic uncertainty in the RICH tagging efficiency has been estimated by using "tight" or "loose" RICH cuts instead of the "standard" ones, and this gives a systematic effect of up to 10%. A 6% error has been added to account for the uncertainty in the overall RICH efficiency. The other systematic errors have been estimated as in section 3.1.5. A summary of the contributions to the systematic errors in the RICH analysis can be found in table 2.

Thus, the total Ω^- production rate found in this analysis is:

Contribution from:	
Background shape	$< \pm$ 1%
Bin width	$\pm$ 4%
Ω^- radial flight cut	$\pm$ 13%
Λ mass cut	$\pm$ 15%
RICH tagging	$\pm$ 10%
RICH efficiency	$\pm$ 6%
JETSET extrapolation I	$\pm$ 9%
JETSET extrapolation II	$\pm$ 9%
Branching ratio $\Omega^- \to \Lambda K^-$	$< \pm$ 1%
Branching ratio $\Lambda \to p\pi^-$	$< \pm$ 1%
Monte Carlo statistics	$\pm$ 3%
Total	$\pm$ 26%

Table 2: Contributions to the systematic error of the Ω^- production rate measured in the RICH analysis.

$$< \Omega^- + \overline{\Omega}^+ > = 0.0012 \pm 0.0004\ (stat.)\ \pm 0.0003\ (syst.)\ .$$

3.3 Combination of the Ω^- measurements

The results of the constrained fit analysis and the RICH analysis are weighted in order to achieve the Ω^- production rate. This weighting recognizes that there are 10 candidate Ω^- decays in common for the two analyses. When evaluating the systematic error of the combined analysis three contributions are added in quadrature: the specific systematics from the two analyses, and the systematics from the cuts shared by the two analyses. These three contributions were equally important. The combined result for the Ω^- production in $q\bar{q}$ events at $\sqrt{s} = 91$ GeV/c^2 is thus found to be

$$< \Omega^- + \overline{\Omega}^+ > = 0.0014 \pm 0.0002\ (stat.)\ \pm 0.0004\ (syst.)\ .$$

4 The Σ^0 Hyperon

The Σ^0 hyperon is identified through the electromagnetic decay $\Sigma^0 \to \Lambda\gamma$ (branching ratio $\sim 100\%$). The Λ is identified through its decay $\Lambda \to p\pi^-$ (branching ratio $\sim 64\%$), while the γ is found only if it converts in the detector, $\gamma \to e^+e^-$.

4.1 Λ selection

Λ candidates are identified using the standard DELPHI V^0 search algorithm as described in section 3.1.1. In addition, particle identification is imposed on the proton candidate in the Λ decay in order to improve the purity of the Λ sample. The criteria for accepting a pair of oppositely charged particles as those coming from a $\Lambda \to p\pi$ decay are that

- the χ^2 probability of the secondary vertex fit exceeds 1%,
- the measured flight in the xy-plane of the Λ candidate exceeds four times its error,
- the angle between the momentum vector of the V^0 and the vector joining the primary and secondary vertices is less than 0.1 rad,

- using TPC and/or RICH information, the charged particle with the highest measured momentum (the proton candidate) is not consistent with the pion hypothesis.

The resulting Λ mass distribution is shown in Figure 7a, together with the corresponding distribution from simulation. The invariant mass of the Λ candidate is required to be within 6 MeV/c^2 of the nominal Λ mass.

4.2 Converted photon reconstruction

The energy spectrum for the photons from $\Sigma^0 \to \Lambda\gamma$ decays peaks at about 150 MeV in the lab frame, which is not a favorable region for reconstruction in the electromagnetic calorimeter. Therefore, the photon selection in this analysis is restricted to those photons which have converted to e^+e^- pairs in material before the TPC. The standard DELPHI converted photon reconstruction is used, and is detailed in this section.

Reconstructed converted photon candidates are found by an algorithm that constrains the line-of-flight of the unseen photons. Requiring that a photon candidate originate at the interaction region, a search is performed on pairs of tracks in the event to find the photon conversion point. Not all tracks are considered, however. Each track individually must contain a point, P, where the tangent to the helix (only the $R\phi$ components of the track are considered) points to the beam spot. The photon conversion radius, or decay point, is defined to be the distance from the interaction point to the point P. Two oppositely charged particles are said to be consistent with a photon conversion if their decay point parameters satisfy the following criteria:

- the reconstructed mean conversion radius (in the $r\phi$ plane) is below 34 cm,
- at least one of the tracks has no associated point in front of the reconstructed mean conversion radius,
- the difference in ϕ between the two conversion points does not exceed 30 mrad,
- the difference between the polar angles θ of the two tracks is smaller than 15 mrad.

For the e^+e^- pairs fulfilling these criteria, a χ^2 is calculated in order to find the best combinations in cases where there are ambiguous associations. A constrained fit is then applied to the electron-positron pair candidate which forces a common conversion point with zero opening angle and collinearity between the momentum sum and the line from the beam spot to the conversion point. Finally, the energy of the conversion electrons is corrected for radiation losses by a small factor that depends on the amount of material between the conversion point and the entrance to the TPC. From simulation, the reconstruction precision of these converted photons has been determined to be 1% in energy, 1.5 mrad in polar and azimuthal angles θ and ϕ, and 5 mm in conversion radius [12].

At very low energies the acceptance drops for asymmetric conversions since the TPC can only reconstruct electrons with a transverse momentum with respect to the beam above 50 MeV/c. The acceptance threshold for converted photons where both the e^+ and the e^- tracks are reconstructed is effectively about 200 MeV.

This conversion reconstruction has also been used for an analysis of the inclusive π^0 cross section [13]. Photon energy and $\gamma\gamma$ invariant mass spectra using conversion pairs have been checked to be in general agreement with the simulation prediction. Figure 7b) shows the mass spectra in data and in the simulated event sample. General agreement is exhibited both in the π^0 peak and the background normalization.

4.3 Σ^0 selection

Those events, for which both a Λ and a γ are reconstructed, have the possibility of containing a Σ^0. The Σ^0 is reconstructed by adding the four-momenta of the Λ and the γ. This is done for every possible $\Lambda\gamma$ combination, yielding a possible Σ^0 candidate. Three cuts are then imposed on the Σ^0, with the effect of increasing the ratio of signal to background. The criteria for selecting Σ^0 candidates are that:

- the Σ^0 energy is between 3 and 15 GeV,
- the cosine of the photon helicity angle (the angle between the photon direction in the Σ^0 rest frame and the flight direction of the Σ^0 in the laboratory frame) is larger than 0,
- the angle of the measured momentum with respect to the beam is between 40° and 140°.

The overall efficiency, after cuts are applied, is calculated using simulation, and then an extrapolation is made to include the entire energy spectrum. There exists some error in extrapolating the measured production rate of the Σ^0 beyond the selected energy range based upon the model used to make that extrapolation. The model-dependence of the Σ^0 energy distribution has been analyzed by comparing the predictions of JETSET 7.4 [14] and HERWIG 5.8 [1] (with JETSET decay modelling), both with default parameters. Comparing these models, a difference is found in the predicted fraction of Σ^0's produced within the selected Σ^0 energy range of 3 to 15 GeV. The JETSET model predicts a softer energy distribution but coincides with HERWIG at around 7.5 GeV. Therefore, what differences exist between the two models tend to cancel both in the measured region, and in the extrapolation. JETSET with DELPHI tuning predicts that 53% of the Σ^0's are produced in the measured range, while HERWIG predicts 52%. The error in extrapolating the measurement to an inclusive production rate for the Σ^0 is estimated to be 5%. The Σ^0 detection efficiency within the measured energy range is calculated from simulation to be $< \varepsilon_{\Sigma^0} > = \ 0.00157 \pm 0.00011\ (stat.)\ \pm 0.00011\ (syst.)$. The systematic error on this value is calculated from quadratic addition of the uncertainties in photon efficiency and the Λ efficiency (7% each).

4.4 Measurement of the Σ^0 production rate

Figure 8a shows the distribution of the difference between the Σ^0 candidate mass and the reconstructed Λ mass in data. Figure 8b shows the distribution from simulation, normalized to the same number of hadronic events as the data. In both figures, there is a clear signal due to $\Sigma^0 \to \Lambda\gamma$ decay. A comparison of the two figures shows that the background shape is well-described by simulation. A nine parameter fit has been performed to the observed distributions, three parameters for the signal and six for the background. The signal is given by a Gaussian and the background is parameterized by $f(m) = (am_b + bm_b{}^2 + cm_b{}^3)e^{(dm_b + em_b{}^2 + fm_b{}^3)}$, where $m_b = m - m_0$ and m_0 is fixed to 0.015 GeV/c^2.

As a check on the resolution of Σ^0 reconstruction and quality of the fit, the mean mass difference between the Σ^0 and the Λ given by the fit procedure may be compared to the well-measured mass difference of 76.9 MeV/c^2 [9]. Both simulation and data are shown to be in good agreement with this value. The fit to the simulation sample gives a peak position at 79.2 ± 0.7 MeV/c^2, with a width of 4.1 ± 0.7 MeV/c^2, and a measured yield of 183 ± 25 Σ^0, statistical error only.

The fit to data is accomplished in two steps. First, the background shape from simulation is used, allowing only the background normalization to vary along with the three peak parameters. This method results in a peak position at 78.0 ± 1.0 MeV/c^2 with a width of 5.4 ± 1.1 MeV/c^2, and shows a yield of 178 ± 26 Σ^0 (Figure 8a). This number will be used in the calculation of the production rate below. The ratio of background normalizations gives a value of 1.01 ± 0.01. Next, all parameters are allowed to vary. The signal region is left out of the fit initially to find the background shape independently. The resulting shape in data is very close to that from simulation background, and gives an estimate of the fit dependence on the fitted background shape and normalization. In this manner, the data signal peak position is found again to be 78.0 ± 1.0 MeV/c^2 with a width of 5.3 ± 1.1 MeV/c^2, and yields 173 ± 25 Σ^0 . The ratio of background normalizations in this method shows a difference of 3% in the signal region. The small difference between the highly-constrained fit in the first step, and the unconstrained fit in the second step, gives us confidence in the ability of the simulation to describe the data accurately.

The dependence of this measurement on the background shape and peak parameters is estimated. Varying the peak position and width within its measured errors causes a $\pm 10\%$ change in the signal and a variation of $\sim 3\%$ is observed when the background is changed between the constrained and unconstrained fits described above. These contributions are included in the systematic error.

Finally, the production rate of Σ^0 in the measured energy range is calculated. Using the efficiency calculated from simulation, the production of Σ^0 per hadronic event is measured to be

$$< \Sigma^0 + \overline{\Sigma}^0 >= 0.037 \pm 0.005 \ (stat.) \ \pm 0.004 \ (syst.) \ .$$

Extrapolation to the entire Σ^0 energy range yields the measured inclusive production rate

$$< \Sigma^0 + \overline{\Sigma}^0 >= 0.070 \pm 0.010 \ (stat.) \ \pm 0.010 \ (syst.) \ .$$

5 Summary

The production rates of the strange baryon Σ^0 and the triply strange baryon Ω^- in the hadronic decay modes of the Z^0 have been measured. The inclusive production rates are determined to be

$$< \Omega^- + \overline{\Omega}^+ >= 0.0014 \pm 0.0002 \ (stat.) \ \pm 0.0004 \ (syst.)$$

$$< \Sigma^0 + \overline{\Sigma}^0 >= 0.070 \pm 0.010 \ (stat.) \ \pm 0.010 \ (syst.) \ .$$

As a comparison, published measurements of Σ^0 and Ω^- production at LEP and at lower energies are summarized in Table 3. In addition, ALEPH and OPAL have presented results on the Ω^- production at the Glasgow (OPAL [4]; $< \Omega >= 0.0028 \pm 0.0009$) and Brussels (ALEPH [5]; $< \Omega >= 0.0010 \pm 0.0003$) conferences.

The prediction of the JETSET 7.3 event generator (with parameters tuned to reproduce DELPHI data [7]) of the Ω^- production rate at LEP energies is 0.0009 Ω^- per hadronic event. This rate is in fair agreement with the present measurement. The HERWIG 5.8

Experiment	ARGUS	MARK II	OPAL	DELPHI
$\sqrt{s}$ [GeV/c^2]	~ 10	~ 30	~ 91	~ 91
$< \Sigma^0 + \overline{\Sigma}^0 >$	0.023 ± 0.008	-	-	0.070 ± 0.014
$< \Omega^- + \overline{\Omega}^+ >$	0.00072 ± 0.00038	0.014 ± 0.007	0.0050 ± 0.0015	0.0014 ± 0.0005
ref	[15]	[16]	[3]	this paper

Table 3: Previously published and present measurements of Σ^0 and Ω^- production in e^+e^- annihilations. Statistical and systematic errors have been added in quadrature.

model (with parameters tuned as in [7]) gives 0.0077 Ω^- per hadronic event which is in clear disagreement with our measurement.

The measured Σ^0 production rate is in good agreement with the JETSET 7.4 model prediction of 0.073. It is also compatible with 1/2 of the measured $\Sigma^\pm$ rate (0.17 ± 0.06) [10], as expected from isospin invariance. The HERWIG 5.8 model predicts a lower production rate of 0.054 for the Σ^0.

Acknowledgements

We are greatly indebted to our technical collaborators and to the funding agencies for their support in building and operating the DELPHI detector, and to the members of the CERN-SL Division for the excellent performance of the LEP collider.

References

[1] G. Marchesini et. al., Computer Physics Communications **67** (1992) 465.
[2] T. Sjöstrand, PYTHIA 5.6 and JETSET 7.3 Physics and Manual, CERN-TH. 6488/92.
[3] OPAL Collaboration, P.D. Acton et al., Phys. Lett. **B291** (1992) 503.
[4] OPAL collaboration, Strange Baryon Production and Correlations in Hadronic Z^0 Decays, Contributed paper n. gls0483 to the ICHEP Conference, Glasgow, Great Britain, 1994.
[5] ALEPH collaboration, Hyperon Production in Z Decays, Contributed paper n. eps0419 to the International Europhysics Conference on High Energy Physics, Brussels, Belgium, July 1995.
[6] DELPHI Collaboration, P. Aarnio et al., Nucl. Instr. and Meth. **A303** (1991) 233.
[7] DELPHI Collaboration, Tuning and Test of Fragmentation Models Based on Identified Particles and Precision Event Shape Data, Contributed paper n. eps0548 to the EPS Conference on High Energy Physics, Brussels, Belgium, July 1995, and Preprint WU B 95-07, Wuppertal (1995).
[8] DELPHI Collaboration, P. Abreu et al., *Performance of the DELPHI detector*, CERN–PPE/95–194, submitted to Nucl. Inst. Meth. A.
[9] Particle Data Group, Phys. Rev. **D50** (1994) 1173.
[10] DELPHI Collaboration, P. Abreu et al., Zeit. Phys. **C67** (1995) 543.
[11] P. Baillon, Nucl. Instr. and Meth **A238** (1985) 341-346.
[12] DELPHI Collaboration, P. Abreu et al., Zeit. Phys. **C68** (1995) 353.
[13] DELPHI Collaboration, W. Adam et al., Measurement of Inclusive π^0 Production in Z Decays, CERN–PPE/95–144, submitted to Zeit. Phys. C.
[14] T. Sjöstrand, Comp. Phys. Comm. **82** (1994) 74.
[15] ARGUS Collaboration, H. Albrecht et al., Zeit. Phys. **C39** (1988) 177.
[16] Mark II Collaboration, S.R. Klein et al., Phys. Rev. Lett. **59** (1987) 2412.

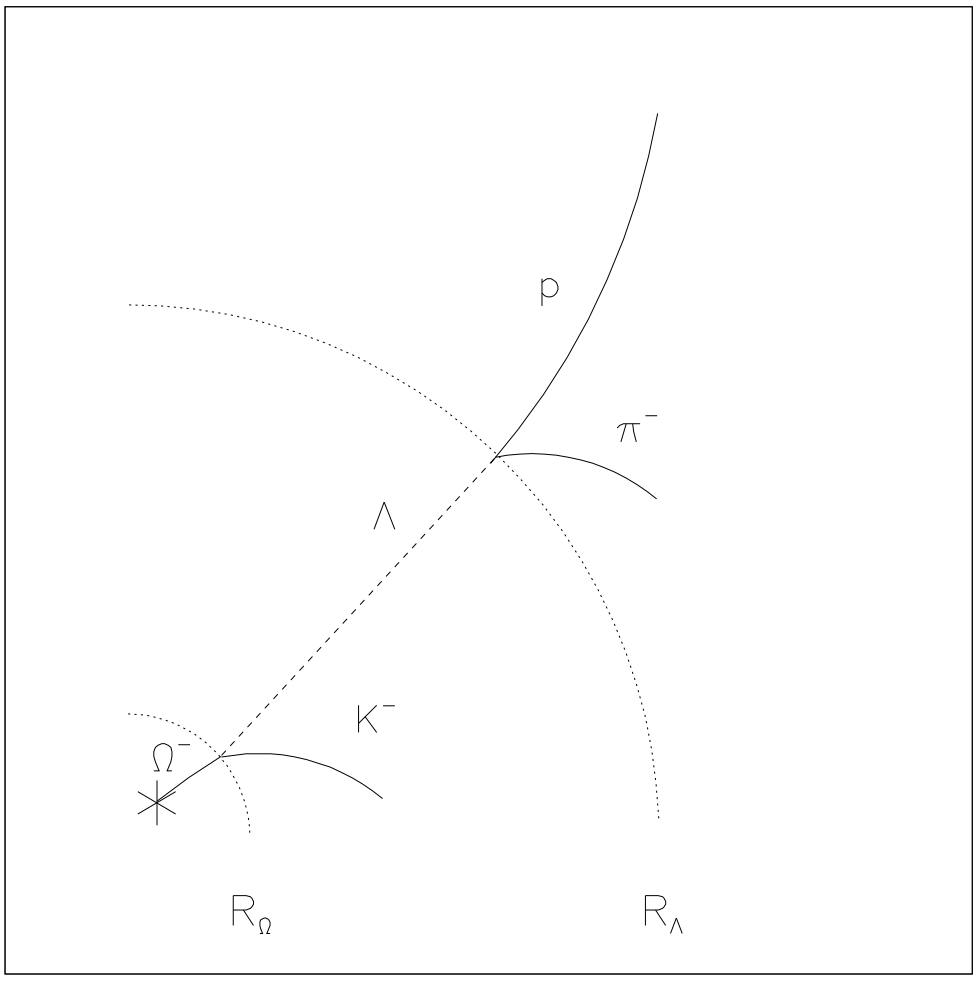

Figure 1: Schematic picture of a Ω^- decay chain. The dotted lines represent the distances of the two decay points. Typical decay radii are a few cm for Ω^- ($c\tau = 2.46$ cm) and in the decimeter range for Λ ($c\tau = 7.89$ cm).

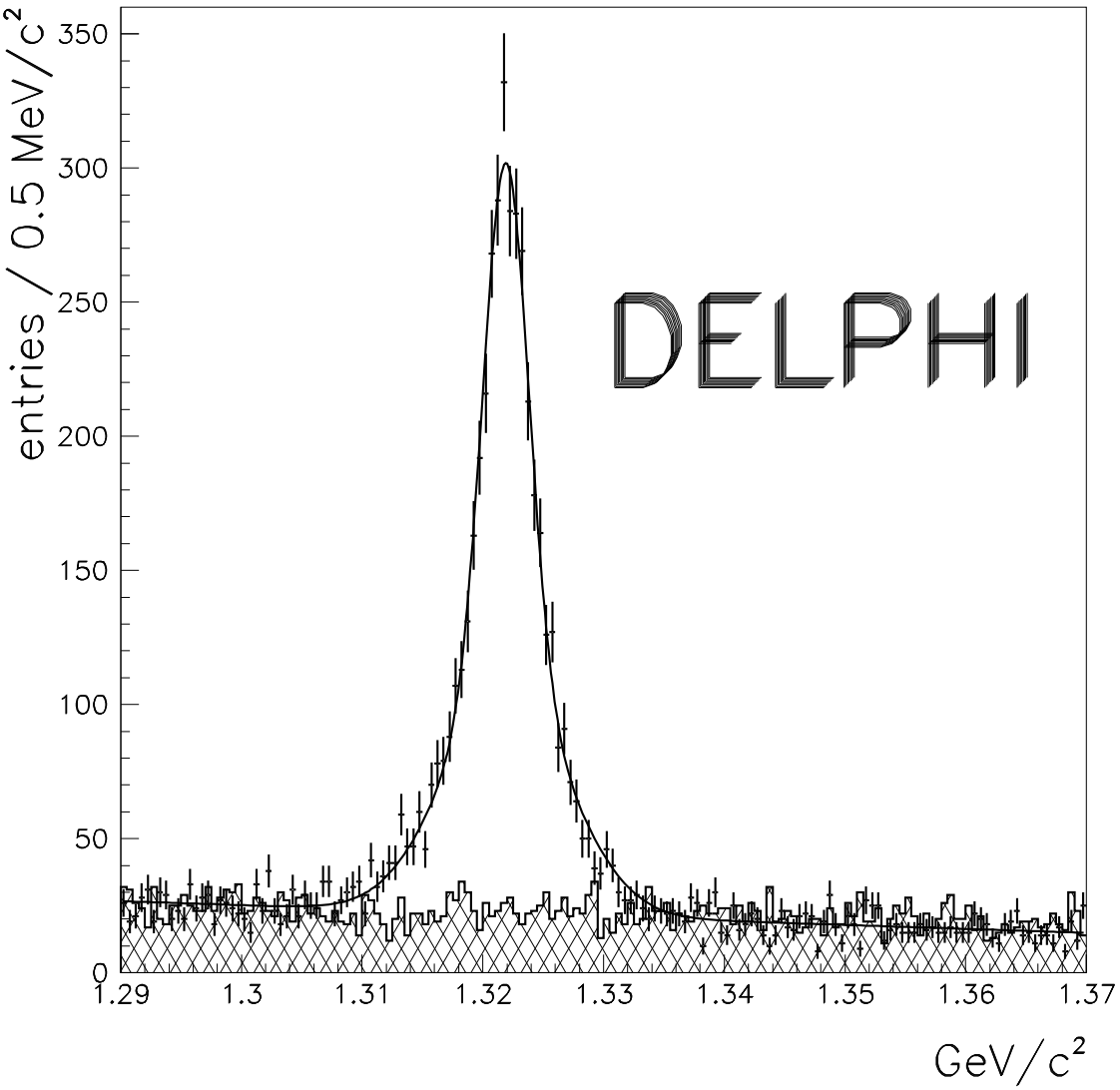

Figure 2: $\Lambda\pi^-$ (and $\bar{\Lambda}\pi^+$) invariant mass spectrum, represented by the points with error bars. The curve is the result of the fit to a sum of two Gaussian distributions with common mean and a linear background. The hatched histogram shows the combinations $\Lambda\pi^+$ and $\bar{\Lambda}\pi^-$ (wrong sign combinations).

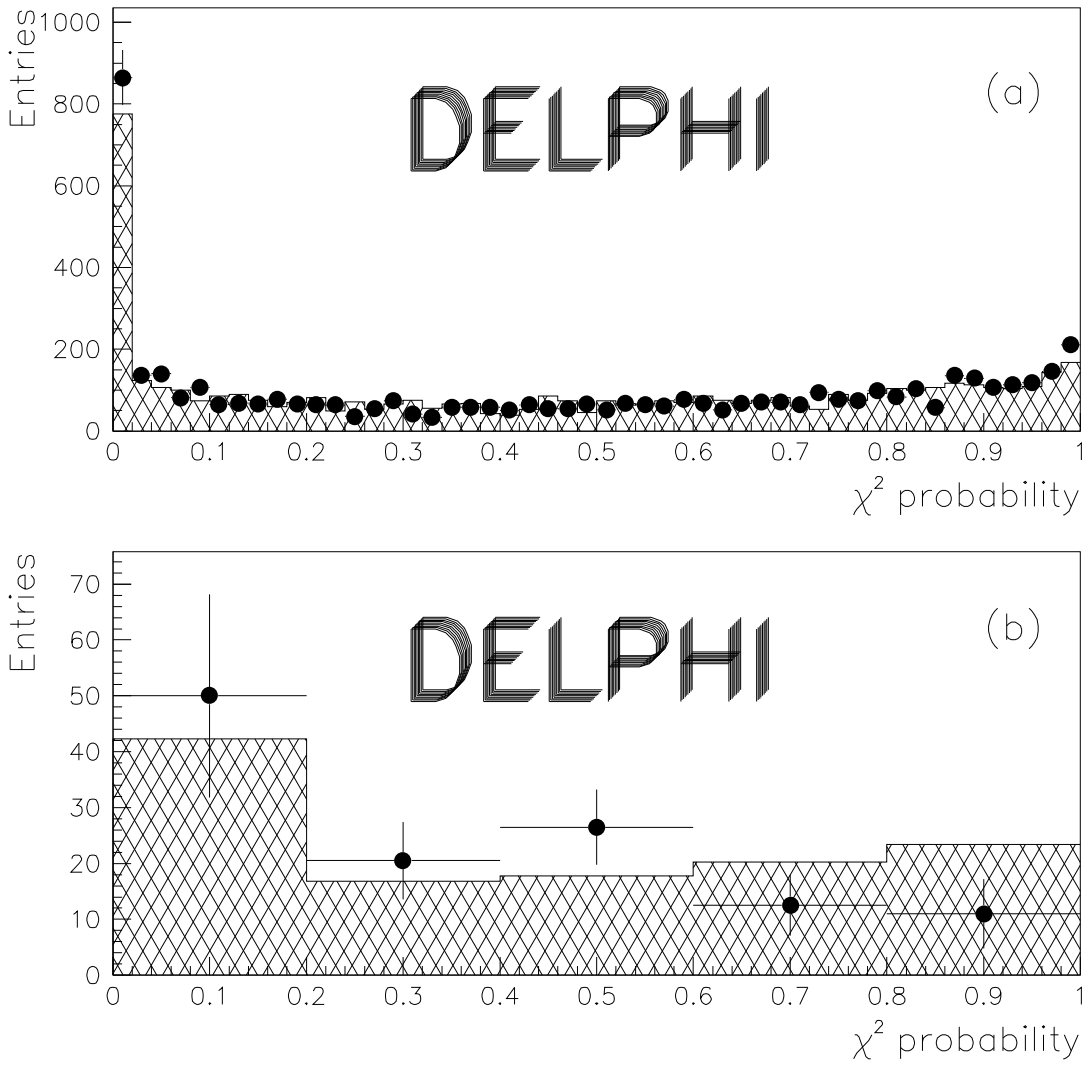

Figure 3: The χ^2 probability distributions of the constrained fit for (a) Ξ^- and (b) Ω^- candidates in data and simulation. All cuts except that on χ^2 probability have been made. The points with error bars are data, and the histograms are from the simulation. Combinatorial background has been subtracted using the wrong sign combinations.

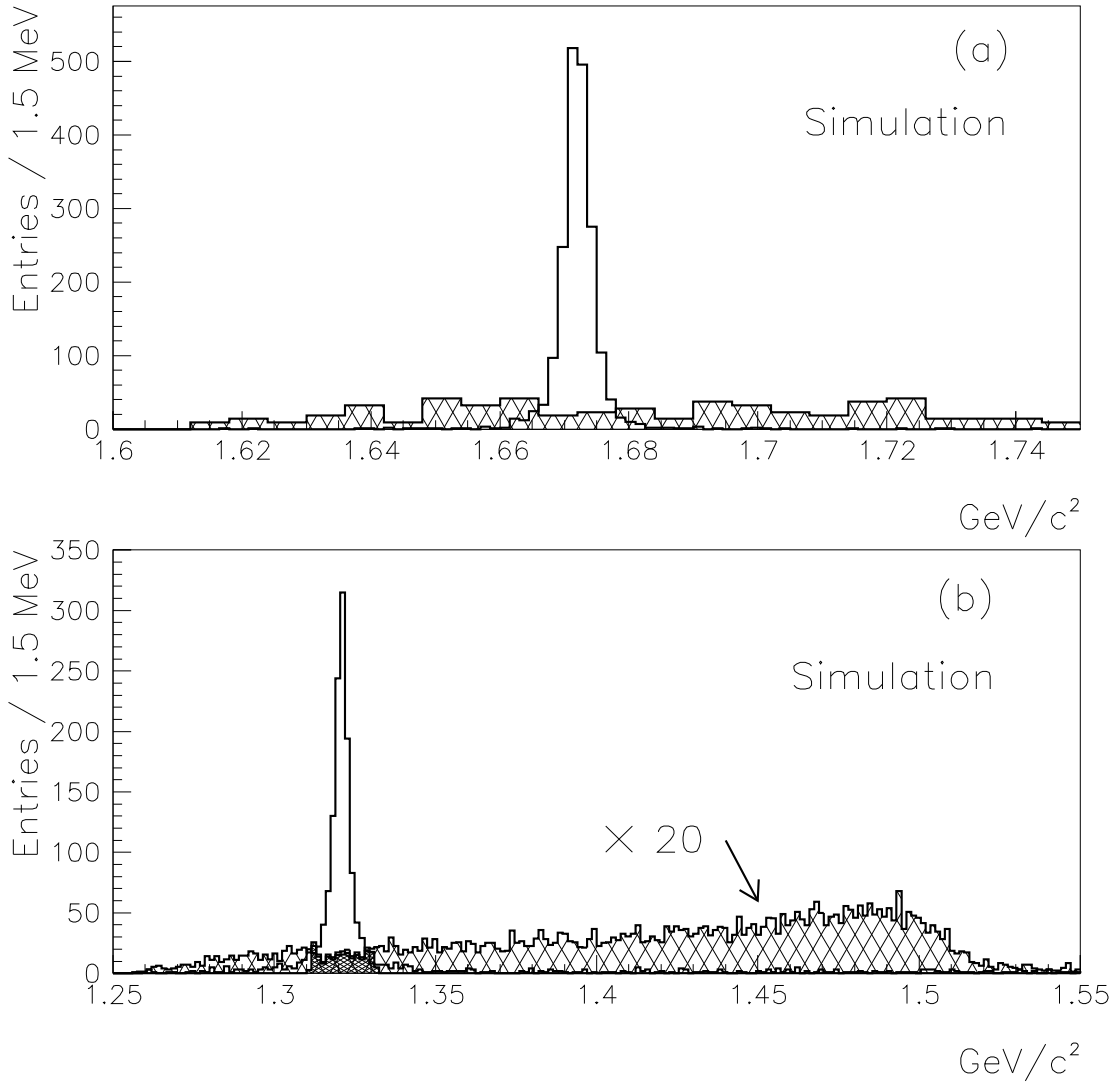

Figure 4: Studies on the reflexions of Ξ^- and Ω^- in simulated events. A ratio of 1:20 of the production rates $<\Omega^->/<\Xi^->$ have been assumed. (a) Ξ^- reflexion under the Ω^- mass peak. The solid line is the Ω^- signal. The hatched histogram is the reflexions from $\Xi^- \to \Lambda\pi^-$ decays, where the pion is treated as a K^-. (b) Ω^- reflexion under the Ξ^- mass peak. The Ω^- reflexion has been magnified a factor 20. The solid line is the Ξ^- signal and the hatched histogram is the reflexion from the decay $\Omega^- \to \Lambda K^-$. The shaded area shows the part of the Ω^- signal lost by requiring the invariant mass in the $\Lambda\pi^-$ hypothesis to lie outside the interval $M_{\Xi^-} \pm 10$ MeV/c^2.

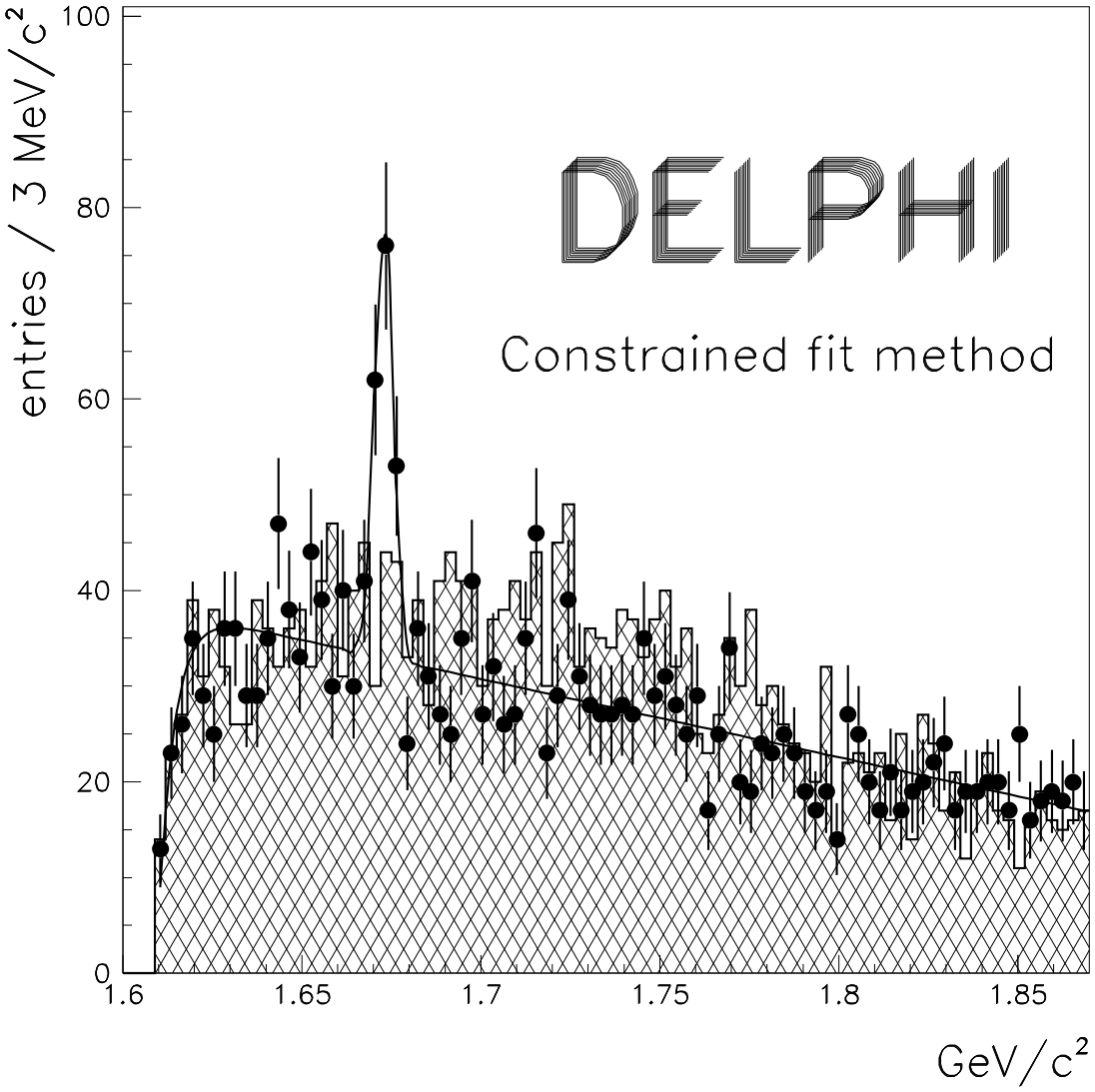

Figure 5: ΛK^- invariant mass spectrum. The points with error bars are the ΛK^- and $\bar{\Lambda} K^+$ combinations. The hatched histogram shows the wrong sign combinations (ΛK^+ and $\bar{\Lambda} K^-$). The line shows the result of the fit described in the text.

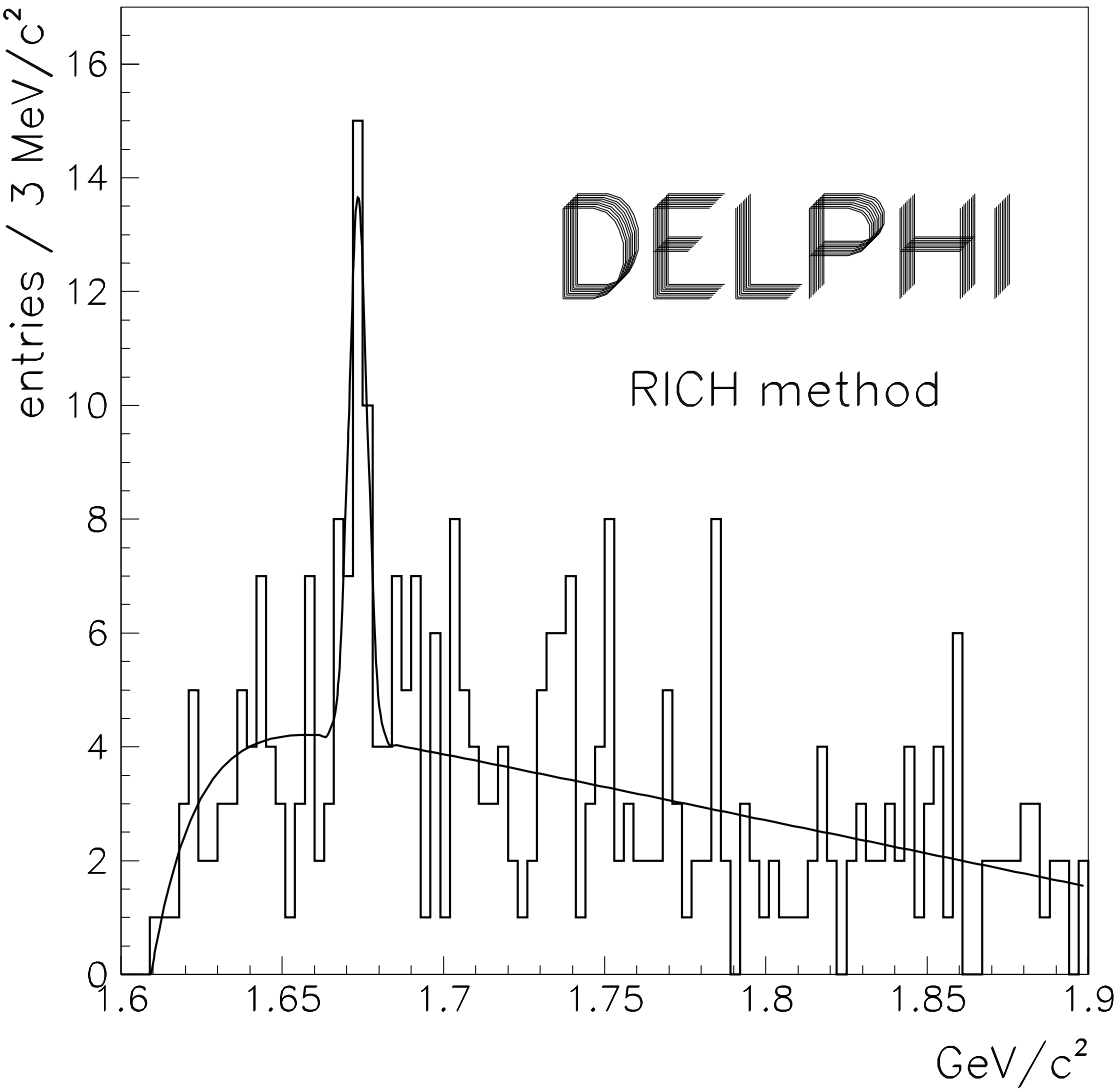

Figure 6: Invariant ΛK^- mass spectrum with the K^- identified with the RICH detector. The line shows the result of the fit described in the text.

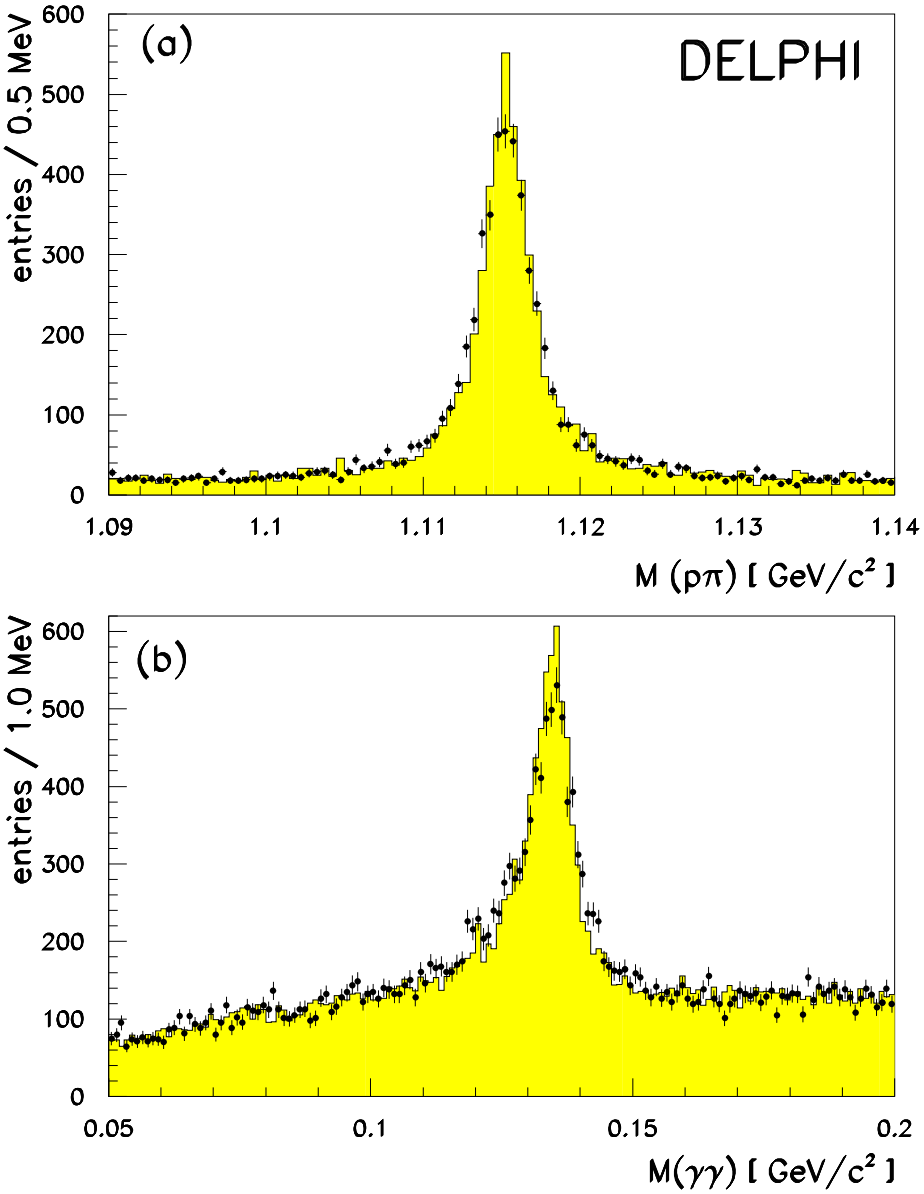

Figure 7: a) The invariant $p\pi$ mass in the Λ region from simulation (histogram) compared to data (points).
b) The invariant $\gamma\gamma$ mass showing the π^0 peak from simulation (histogram) compared to data (points).

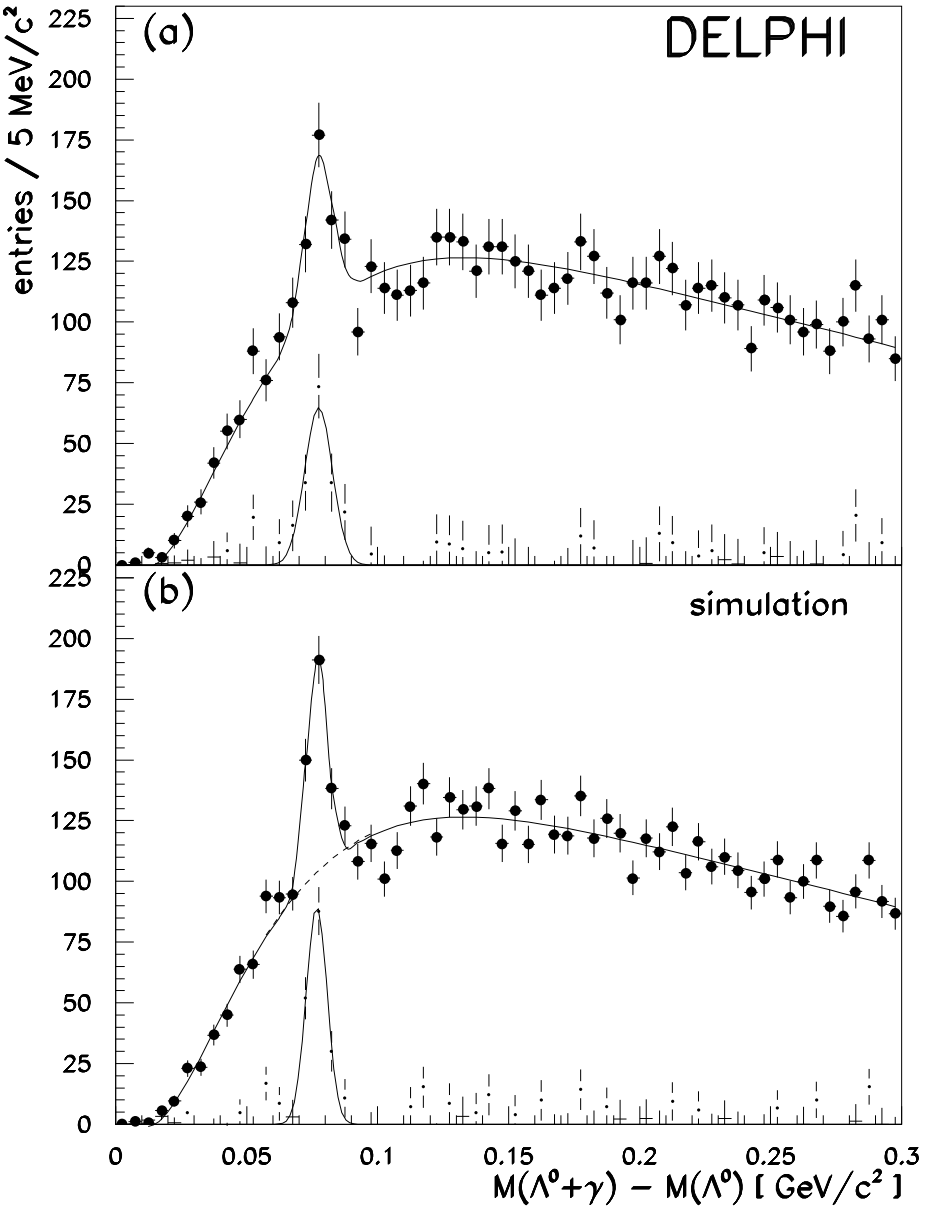

Figure 8: $\Lambda\gamma$ - Λ mass difference distribution.
a) The data are shown by points with error bars; the line corresponds to the fit with background shape from simulation. The insert shows the background-subtracted histogram.
b) The simulation is shown by points with error bars; the solid line corresponds to the fit. The dashed line shows the fit to background only. The points with the small dots show the background-subtracted distributions.